TITLE: **Preliminary evaluation of the impact of temperature fluctuations in the HFI 4K-stage on LFI**

DOC. TYPE: TECHNICAL NOTE

PROJECT REF.: PL-LFI-PST-TN-048 **PAGE:** I of V, 13

ISSUE/REV.: Issue 1.0 **DATE:** September 2003

Prepared by	L. TERENZI A. MENNELLA L. VALENZIANO G. MORGANTE D. MAINO M. PRINA M. BERSANELLI M. TOMASI LFI System Team	Date: September 6th, 2003 Signature:
Agreed by	C. BUTLER LFI Program Manager	Date: September 6th, 2003 Signature:
Approved by	N. MANDOLESI LFI Principal Investigator	Date: September 6th, 2003 Signature:

DISTRIBUTION LIST

Recipient	Company / Institute	E-mail address	Sent
T. PASSVOGEL	ESA – Noordwijk	tpassvog@estec.esa.nl	Yes
G. CRONE	ESA – Noordwijk	Gerald.Crone@esa.int	Yes
J. MARTI-CANALES	ESA – Noordwijk	Javier.Marti.Canales@esa.int	Yes
M. VON HOEGEN	ESA – Noordwijk	mvhoegen@estec.esa.nl	Yes
P. OLIVIER	ESA – Noordwijk	Pierre.olivier@esa.int	Yes
J. TAUBER	ESA – Noordwijk	jtauber@astro.estec.esa.nl	Yes
B. COLLAUDIN	ALCATEL – Cannes	bernard.collaudin@space.alcatel.fr	Yes
J.P. CHAMBELLAND	ALCATEL – Cannes	Jean-Philippe.Chambelland@space.alcatel.fr	Yes
N. MANDOLESI	IASF/CNR – Bologna	reno@bo.iasf.cnr.it	Yes
C. BUTLER	IASF/CNR – Bologna	butler@bo.iasf.cnr.it	Yes
A. MENNELLA	IASF/CNR – Milano	daniele@mi.iasf.cnr.it	Yes
M. TOMASI	IASF/CNR – Milano	zio_tom78@hotmail.com	Yes
L. VALENZIANO	IASF/CNR – Bologna	valenziano@bo.iasf.cnr.it	Yes
G. MORGANTE	IASF/CNR – Bologna	morgante@bo.iasf.cnr.it	Yes
F. VILLA	IASF/CNR – Bologna	villa@bo.iasf.cnr.it	Yes
L. TERENZI	IASF/CNR – Bologna	terenzi@bo.iasf.cnr.it	Yes
M. BERSANELLI	UniMi – Milano	marco@mi.iasf.cnr.it	Yes
D. MAINO	UniMi – Milano	davide.maino@mi.infn.it	Yes
F. PASIAN	OAT – Trieste	pasian@oat.ts.astro.it	Yes
E. ALIPPI	LABEN – Vimodrone	alippi.e@laben.it	Yes
A. DRAGONI	LABEN – Vimodrone	dragoni.a@laben.it	Yes
M. MICCOLIS	LABEN – Vimodrone	miccolis.m@laben.it	Yes
L. PAGAN	LABEN – Vimodrone	pagan.l@laben.it	Yes
M. DE PAOLI	LABEN – Vimodrone	depaoli.m@laben.it	Yes
E. ARTAL	Univ. of Cantabria – Santander	artal@dicom.unican.es	Yes
R. DAVIS	Jodrell – UK	rjd@jb.man.ac.uk	Yes
A. WILKINSON	Jodrell – UK	aw@jb.man.ac.uk	Yes
C. LAWRENCE	JPL – Pasadena	crl@jplsp.jpl.nasa.gov	Yes
M. PRINA	JPL – Pasadena	mauro@squid.jpl.nasa.gov	Yes
T. GAIER	JPL – Pasadena	gaier@merlin.jpl.nasa.gov	Yes
M. SEIFFERT	JPL – Pasadena	Michael.d.seiffert@jpl.nasa.gov	Yes

S. LEVIN	JPL – Pasadena	steve@beta.jpl.nasa.gov	Yes
P. BHANDARI	JPL – Pasadena	Pradeep.Bhandari@jpl.nasa.gov	Yes
L. WADE	JPL – Pasadena	lawrence.a.wade@jpl.nasa.gov	Yes
R. HOYLAND	IAC - Tenerife	rjh@ll.iac.es	Yes
J. TUOVINEN	Millilab – Finland	Jussi.tuovinen@vtt.fi	Yes
J.L. PUGET	IAS – Orsay	puget@ias.u-psud.fr	Yes
J-M. LAMARRE	LERMA – Paris	lamarre@ias.u-psud.fr	Yes
J-J. FOURMOND	IAS – Orsay	fourmond@ias.u-psud.fr	Yes
G. GUYOT	IAS – Orsay	guyot@ias.u-psud.fr	Yes
J. FEREDAY	RAL – Chilton (UK)	j.fereday@rl.ac.uk	Yes
T. BRADSHAW	RAL – Chilton (UK)	Tom.Bradshaw@rl.ac.uk	Yes
R. EMERY	RAL – Chilton (UK)	r.j.emery@rl.ac.uk	Yes
LFI System PCC	TESRE – Bologna	lfispcc@tesre.bo.cnr.it	Yes
Radiometer WG		rwg@beta.jpl.nasa.gov	Yes

CHANGE RECORD

Issue	Date	Sheet	Description of Change	Release
Issue 1.0	Sept '03	All	First issue of document	1.0

Abstract

In this technical note we provide a preliminary analysis of the effect of temperature fluctuations at the level of the HFI 4K stage on the scientific performances of the Planck-LFI instrument. The stability of this stage is of crucial importance for the LFI, as it impact directly the stability of the measured signal through its reference load. The availability of the first simulations of the 4K temperature stability from the HFI team has prompted a quick assessment of the expected effect, which is found to be large enough to require the application of software removal algorithms to maintain the residual effect in the final maps within the required levels. Clearly it is of crucial importance the availability in a short time of measurements from the HFI 4K cooler in order to be able to perform robust estimates of the final expected systematic effect.

1. Introduction

The Planck-LFI radiometric receivers are pseudo-correlation radiometers [1, 2] that continuously compare the sky signal with a stable reference signal in order to minimise the effects from gain instabilities. This reference signal is provided by ECCOSORB loads thermally linked to the HFI 4K stage [3] which must display a high degree of stability to maintain at a μK level in the final maps any spurious signal caused by such instabilities.

1.1 4K Reference Load Implementation

70 GHz loads are mounted on the upper part of the HFI cryostat. They are bonded to a mounting structure facing the 6 LFI 70 GHz FEMs. 30 and 44 GHz loads are located on the cylindrical part of the HFI cryostat. They are mounted in individuals mounting structures. These latter loads are closer to the 4K cooler cold end and are probably the most affected by temperature fluctuations.

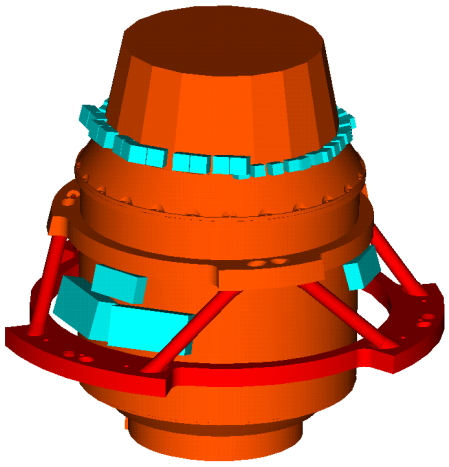

Figure 1 –Loads location on the HFI cryostat. Small blue blocks on the upper sector (100 GHz loads) are not present anymore

1.2 Temperature stability requirements

The stability requirements of the reference load temperature have been specified in [4] and are summarised in the table below:

Table 1 – Required stability of the temperature of the LFI 4K reference loads

Random fluctuations (high frequencies, > 1 Hz)	Spin-synchronous fluctuations	Periodic fluctuations (non spin-synchronous, low frequencies < 1 Hz)
10 mK/Hz$^{1/2}$	± 1 μK	± 1 mK

The temperature stability at the level of the reference loads is the result of temperature fluctuations propagating from many sources through the HFI instrument to the loads located on the external shield of the HFI box:

- temperature fluctuations at the LR2/LFI interface that propagate to the HFI instrument through the struts connecting the HFI to the LFI;
- temperature fluctuations at the LR1/HFI interface propagating from the 18 K plate to the 4 K cold end;
- temperature fluctuations at the 4 K cold end propagating through the 4 K box to the LFI reference loads.

Furthermore we must take into account that the temperature stability of the various cold ends are not independent; in fact the stability of the LR1 cold end depends on the stability of the LR2 cold end and the stability of the 4 K cooler itself depends on the stability of the temperature of the 18 K stage.

Recently the HFI team has made available estimations of the temperature stability at some interface points between the 4 K box and the reference loads considering the temperature behaviour of the LR1 cold end. This behaviour has been derived from the latest tests on the EBB Sorption Cooler in which a PID active control was implemented to stabilise the temperature at the LR2/LFI interface. The propagation of the resulting temperature oscillations through the ECCOSORB targets has been implemented by means of a simplified thermal model. In this note we report preliminary estimations of the effect of such temperature instabilities for a 30 GHz and a 70 GHz channel case.

The results show that the effect cannot be considered negligible although is not at a *show-stopper* level. Further investigations are needed (i) to evaluate the effect of temperature fluctuations of the 4K cooler itself, (ii) to evaluate the effect on maps and power spectra also considering the presence of various astrophysical signals and instrumental noises, and (iii) to model more accurately the signal emitted by the reference load into the radiometer as a consequence of physical temperature fluctuations.

2. Sources of thermal instability

In this study only the sorption cooler cold-ends LR1 and LR2 have been considered as sources of temperature oscillations. Therefore the temperature fluctuations at the level of the 4 K cooler neglect any possible contribution from instabilities intrinsic to the 4 K cooler itself. The input data of temperature versus time at the 18 K and 20 K stages come from a set of measurements performed on the Sorption Cooler EBB in which the LR2/LFI interface was stabilized with an active PID controller implemented according two different scenarios: (i) Coupled Design and (ii) Uncoupled Design. These different setups refers to a thermal link between the PID stage and LR3 on the sorption cooler cold end and don't differ significantly for their impact upon LR1 stabilty. For further regarding the controller implementation see [5, 6].

In Figure 2 we show the measured temperature at the LR2 cold end with the two implementations of the PID controller, while in Figure 3 we report the corresponding amplitude spectra.

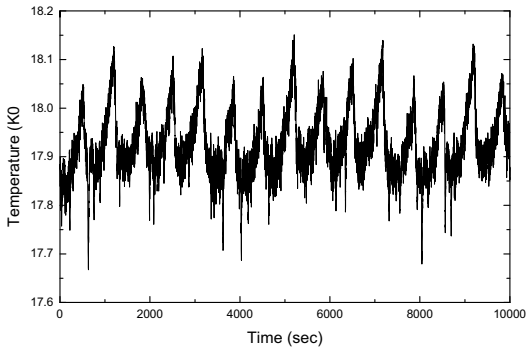

(a)

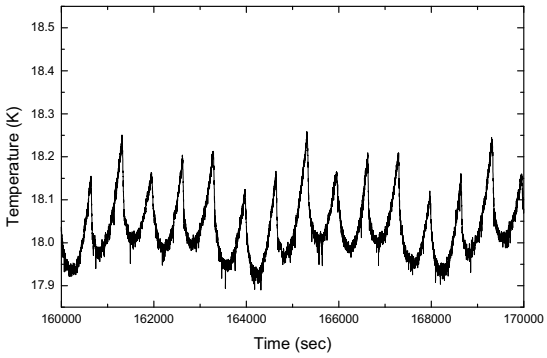

(b)

Figure 2 – Temperature at the LR1 cold end of the EBB Sorption Cooler with active stabilisation of the temperature at the LR2/LFI interface; (a) PID controller with "Coupled" design, (b) PID controller with "Uncoupled" design

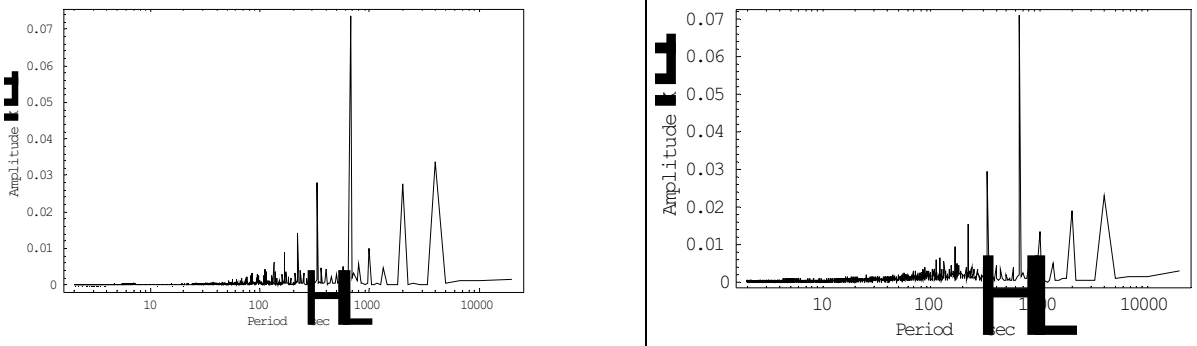

(a) (b)

Figure 3 – Amplitude spectrum of the temperature fluctuations at the LR1 cold end of the EBB Sorption Cooler with active stabilisation of the temperature at the LR2/LFI interface; (a) PID controller with "Coupled" design, (b) PID controller with "Uncoupled" design

3. Propagation of temperature fluctuations from LR1 to the LFI reference loads

In [7] it has been reported a thermal simulation study with the aim to evaluate the transfer function (f_{trans}) characterising the propagation of temperature fluctuations from the LR1 cold end to the 4 K box. The transfer function is such that for each position $\vec{x}$ on the 4 K box the amplitude of a temperature fluctuation having frequency ν and phase ϕ can be calculated as:

$$\Delta T(\vec{x}, \nu, \phi) = f_{\text{trans}}(\vec{x}, \nu, \phi) \times \Delta T_{\text{LR1}}(\nu, \phi) \quad (1)$$

In Figure 4 we show the amplitude transfer function relative to a 30 GHz channel reference load, which represents the most sensitive reference load to temperature fluctuations at the LR1 (see discussion in Sec.1.1). In our treatment we have neglected the phase contribution to the transfer function, as it was not evaluated in the HFI study.

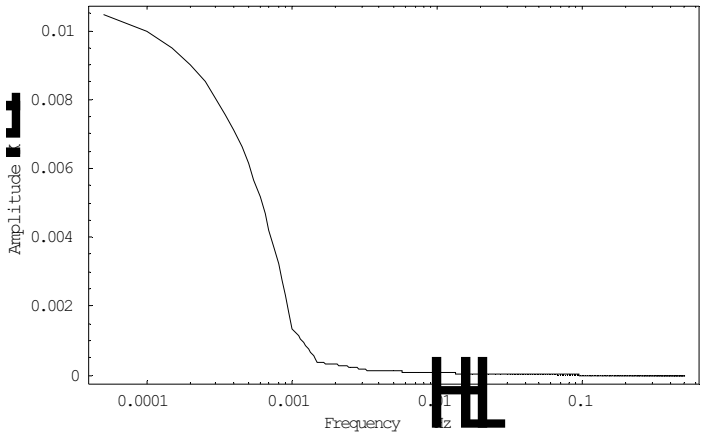

Figure 4 – Amplitude transfer function for the propagation of temperature fluctuations from the LR1 cold end to the reference load.

We have also evaluated the thermal damping provided by the ECCOSORB loads using a 2-D analytical thermal model [8]; in Figure 5 we show the result relative to a 30 GHz ECCOSORB target, which shows that the thermal damping provided by the loads themselves is negligible compared to the overall thermal damping (cfr. with Figure 4).

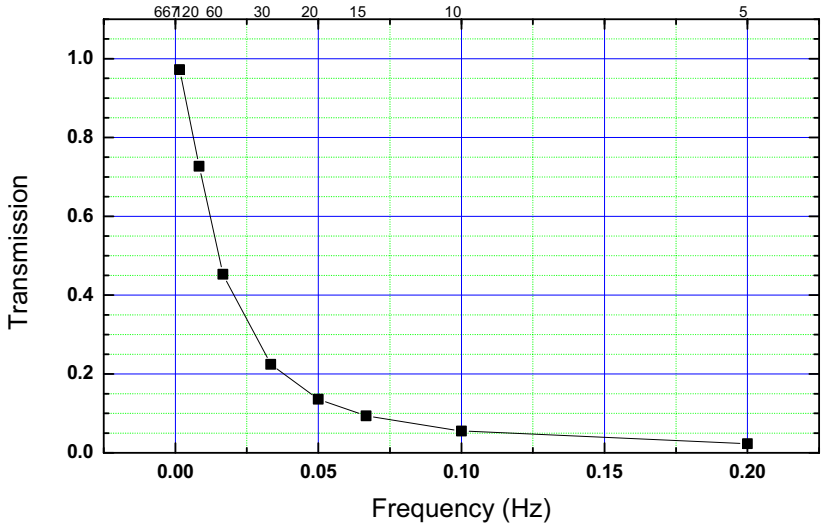

Figure 5 – Amplitude transfer function for the propagation of temperature fluctuations through a 30 GHz LFI reference load.

4. Measured signal instability

The next step is to convert the physical temperature fluctuation of the reference target first into a variation of the radiometer reference signal and ultimately into a variation of the measured signal.

Assuming perfect emissivity for the reference target we can approximate the variation of the reference signal in antenna temperature, ΔT_A caused by a variation in physical temperature, $\Delta T_{\rm phys}$, by $\Delta T_A = \frac{x^2 e^x}{\left(e^x - 1\right)^2} \delta T_{\rm phys} \equiv \eta \times \delta T_{\rm phys}$, where $x = \frac{h\nu}{kT_0}$ and, in our case, $T_0 \sim 4.5$ K.

The radiometric transfer function can be calculated considering the differential radiometer output power defined as:

$$p(t) = ak\beta G_{\rm FE} G_{\rm BE} G_{\rm DC} \left[\widetilde{T}_{\rm sky} + T_{n_{\rm FE}} + \frac{T_{n_{\rm BE}}}{G_{\rm FE}} - r\left(\widetilde{T}_{\rm 4K} + T_{n_{\rm FE}} + \frac{T_{n_{\rm BE}}}{G_{\rm FE}} \right) \right] \qquad (2)$$

where:

- $\widetilde{T}_{\rm sky} = \frac{T_{\rm sky}}{L_{\rm feed-OMT}} + \left(1 - \frac{1}{L_{\rm feed-OMT}}\right) T_{\rm phys}$ represents the sky signal at the output of the feed-OMT system,
- $\widetilde{T}_{\rm 4K} = \frac{T_{\rm 4K}}{L_{\rm 4K}} + \left(1 - \frac{1}{L_{\rm 4K}}\right) T_{\rm phys}$ represents the reference signal at the output of the reference horns,
- $T_{\rm phys}$ is the temperature of the front end (~20 K),
- the L parameters represent the insertion losses of the front-end passive components,
- the G parameters represent gains of the RF and DC amplifiers,
- the $T_{\rm n}$ parameters represent the front-end and back-end amplifier noise temperatures,
- $r \approx \frac{\widetilde{T}_{\rm sky} + T_{\rm sys}}{\widetilde{T}_{\rm 4K} + T_{\rm sys}}$ is the gain modulation factor,
- β is the radiometer bandwidth, k the Boltzmann constant and a is the proportionality constant of the square law detectors.

In Table 2 we summarise the baseline radiometer parameters used in our calculations.

Table 2 – Baseline radiometer parameters

Frequency (GHz)	30	44	70
η	0.991513	0.98185	0.95482
$L_{\text{feed-OMT}}$ (dB)	0.25	0.25	0.25
L_{4K} (dB)	0.2	0.2	0.2
G_{FE}(dB)	35	35	35
G_{BE}(dB)	35	35	35
$T_{n_{FE}}$(K)	8.60	14.10	25.70
$T_{n_{BE}}$(K)	350	350	450
T_{phys}(K)	20	20	20
r	0.8235	0.8721	0.9214

If we denote with $\delta T_{\text{rad}}^{4K}$ the variation in the radiometer output caused by a variation δT^{4K} in the reference load signal we can write $\delta T_{\text{rad}}^{4K} = TF_{\text{rad}}^{4K} \cdot \delta T^{4K}$ where $TF_{\text{rad}}^{4K} = \left(\frac{\partial p}{\partial T_{\text{sky}}}\right)^{-1} \frac{\partial p}{\partial T_{4K}} \delta T^{4K} = -r \frac{L_{\text{feed-OMT}}}{L_{4K}}$.

In Figure 6 we show an example of the differential output of a 30 GHz radiometer caused by a fluctuation in the reference signal induced by temperature oscillations at the LR1 cold end (coupled scenario, see Figure 2-a). The peak-to-peak effect at this level is of the order of ~ 0.6 mK.

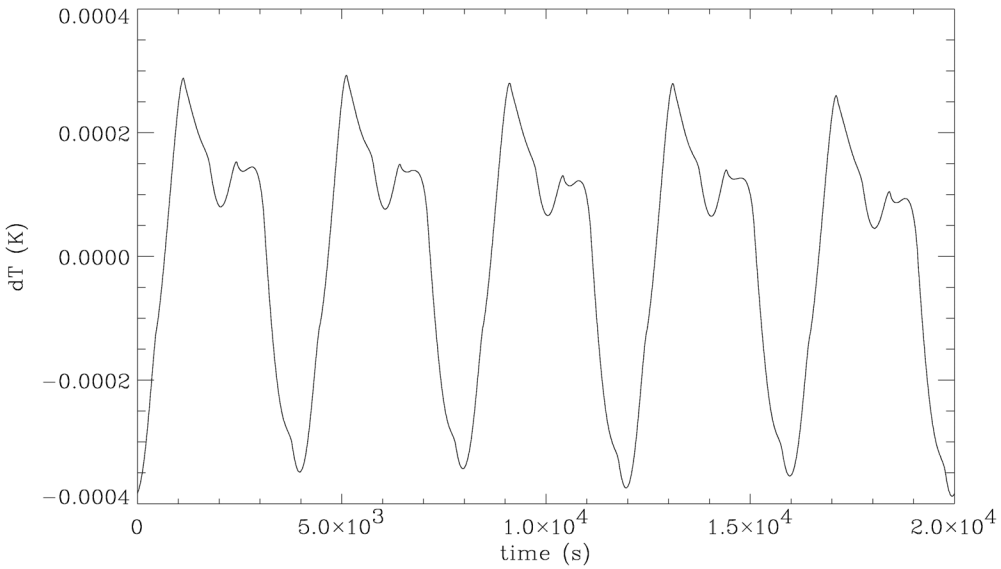

Figure 6. Time ordered data representing the 30 GHz radiometric output caused by a fluctuation in the 4 K reference signal induced by LR1 temperature variations (coupled scheme, see Figure 2).

In Figure 7 we show the amplitude spectrum of the above data stream, from which it is apparent that the fluctuation is dominated by slow harmonics (with frequency < 1 mHz). In particular the right panel shows that the spin synchronous components are expected to be at sub-μK level.

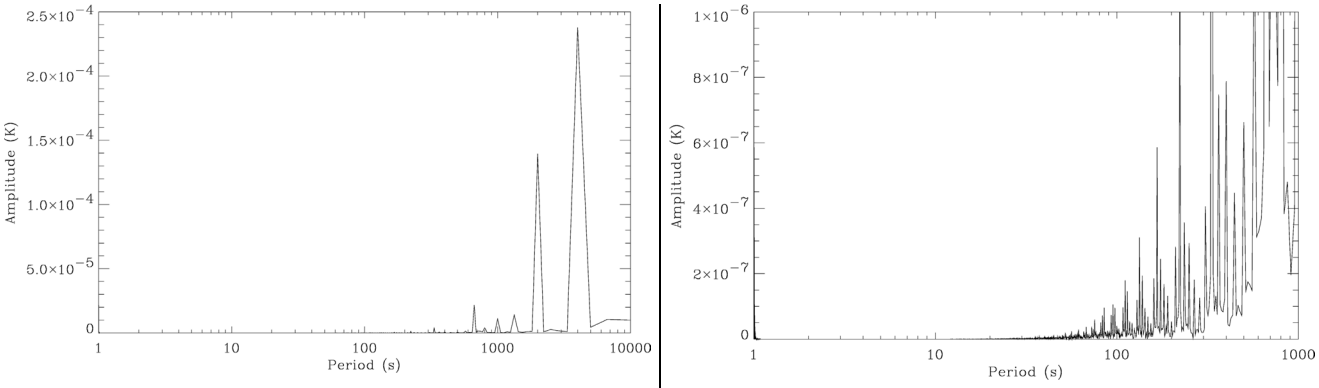

(a) (b)

Figure 7 – Amplitude spectrum of the data stream in Figure 6. The right panel represents an expansion of the high frequency part of the spectrum

5. Estimate of the peak-to-peak effect on the final maps

5.1 Analytical treatment

Under quite general assumptions the peak-to-peak effect of periodic oscillations in the detected signal on the reconstructed sky map can be evaluated analytically [9]. In fact if we consider a periodic fluctuation (δT) of general shape in the detected signal, we can expand it in Fourier series, i.e.: $\delta T = \sum_{j=-\infty}^{+\infty} A_j \exp(i\, 2\pi\, \nu_j\, t)$, where ν_j represents the different frequency components in the fluctuation.

Let us now estimate what is the damping factor for the various harmonics determined by the measurement strategy alone. To do this we consider two different regions of the frequency spectrum with respect to the satellite spin frequency, ν_{spin}:

- the **low frequency region**, i.e. $\nu_j < \nu_{spin}$, and
- the **high frequency region,** i.e. $\nu_j \geq \nu_{spin}$.

In the low frequency region each harmonic with amplitude A_j will be damped by the measurement redundancy and by the projection of the time ordered data onto a map with a pixel size θ_{pix} by a factor proportional to $\sin(\pi\, \nu_j/\nu_{spin})$. In the high frequency region, instead, we make a distinction between frequencies that are synchronous with the spin (i.e. $\nu_j = k\, \nu_{spin}$) and frequencies that are not (i.e. $\nu_j \neq k\, \nu_{spin}$). For the first ones there will be no damping effects as these signals are practically indistinguishable from the

sky measurement, while the second will be damped by a factor of the order of $N \times \theta_{pix} / \theta_{rep}$ where θ_{rep} represents the satellite repointing angle (i.e. the angle between two consecutive scan circles in the sky).

Besides the damping provided by the measurement redundancy we can also add an additional reduction provided by the application of high-pass filtering algorithms to the time ordered data: if we denote with F_j this additional damping then we can write the following expression of the final peak-to-peak effect of a generic signal fluctuation δT on the map:

$$\left\langle \delta T^{\text{p-p}} \right\rangle_{\text{map}} \approx 2\left[\frac{1}{N \times \theta_{\text{pix}} / \theta_{\text{rep}}} \left(\sum_{\nu_j < k\,\nu_{\text{spin}}} \left| \frac{A_j / F_j}{\sin(\pi \nu_j / \nu_{\text{spin}})} \right| + \sum_{\substack{\nu_j < \nu_{\text{spin}} \\ \nu_j \neq \nu_{\text{spin}}}} \left| A_j / F_j \right| + \sum_{\nu_j = \nu_{\text{spin}}} \left| A_j \right| \right) \right] \tag{3}$$

where N is the number of times each sky pixel is sampled during each scan circle.

5.2 Analytical estimates results

In the following tables (Table 3 and Table 4) we report a summary of the peak-to-peak effects on the final maps estimated with the analytical method outlined in Section 5.1. The estimation has been done both considering a pixel size equal to the physical beam size (see results in Table 3) and considering a pixel size relative to the N_{side} parameter that is used to build the maps (i.e. N_{side}= 256 at 30 and 44 GHz and N_{side} = 512 at 70 GHz).

The results shown in the following tables show that the estimated effect is in the range of 1 – 2 μK depending on the frequency, which is close to the maximum allowed systematic error from reference load fluctuations as specified in the systematic error budget [4] especially at 70 GHz, where the effect has a greater impact because of the smaller pixel size.

Table 3 – Estimated peak-to-peak effect on map with pixel sizes corresponding to the physical beam size

	30		44		70	
Pixel size (arcmin)	33		24		14	
	Before destriping	After destriping	Before destriping	After destriping	Before destriping	After destriping
Coupled scheme	23.78	0.90	34.32	1.32	60.51	2.34
Uncoupled scheme	22.42	0.77	32.38	1.13	57.16	2.06

Table 4 – Estimated peak-to-peak effect on map with pixel sizes corresponding to the map N_{side} parameter

	30		44		70	
Pixel size (arcmin)	13.7		13.7		6.8	
	Before destriping	After destriping	Before destriping	After destriping	Before destriping	After destriping
Coupled scheme	57.29	2.18	60.13	2.30	123.67	4.79
Uncoupled scheme	54.00	1.85	56.73	1.98	116.83	4.23

5.3 Maps and power spectra

In this section we show some examples of maps and power spectra calculated using the time streams relative to the coupled scenarios for the 30 and 70 GHz cases.

In Figure 8 we show maps relative to the 30 GHz channel (in ecliptic coordinates) of the effect before and after classical destriping was applied. Because the classical destriping algorithm removes constant offsets from every (coadded) ring the residual effect on the destriped map is not spread uniformly over the map, but has a higher amplitude on one half of the map compared to the other. Tests are in progress using a generalised version of the destriping algorithm which is able to remove more complex functions from time ordered data (e.g. linear slopes).

Note that the peak-to-peak effect calculated on the maps (before and after destriping) is in agreement with the analytical estimates summarised in

Table 4.

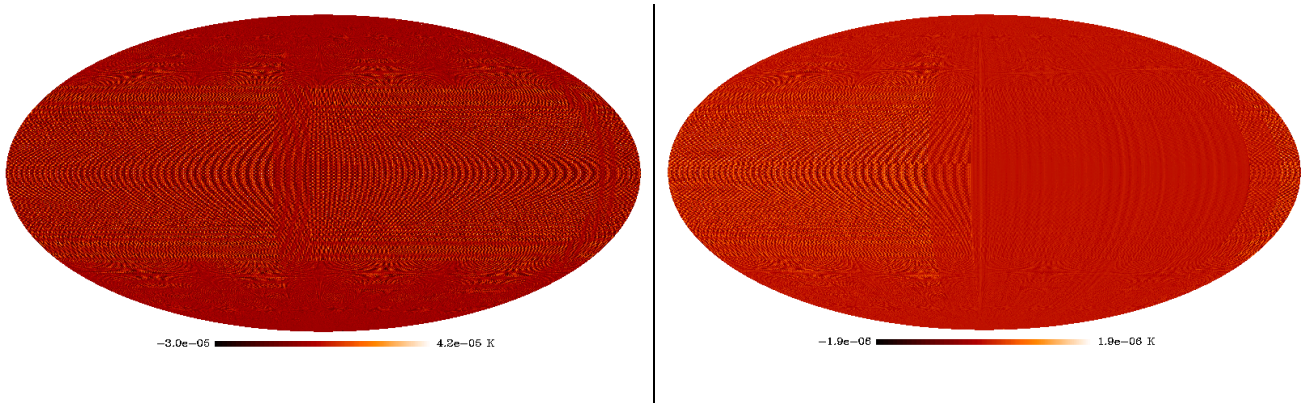

Figure 8 – Maps before and after destriping of the effect induced by fluctuations of the 4K reference load in the coupled scenario at 30 GHz

In the following figure power spectra of the effect before and after destriping are compared to a typical CMB power spectrum; while the power spectrum of the effect before exceeds the CMB at multipoles $l > 450$, the power spectrum of the effect after destriping is at least two order of magnitudes less than the CMB power spectrum (also for low values of l, see inset).

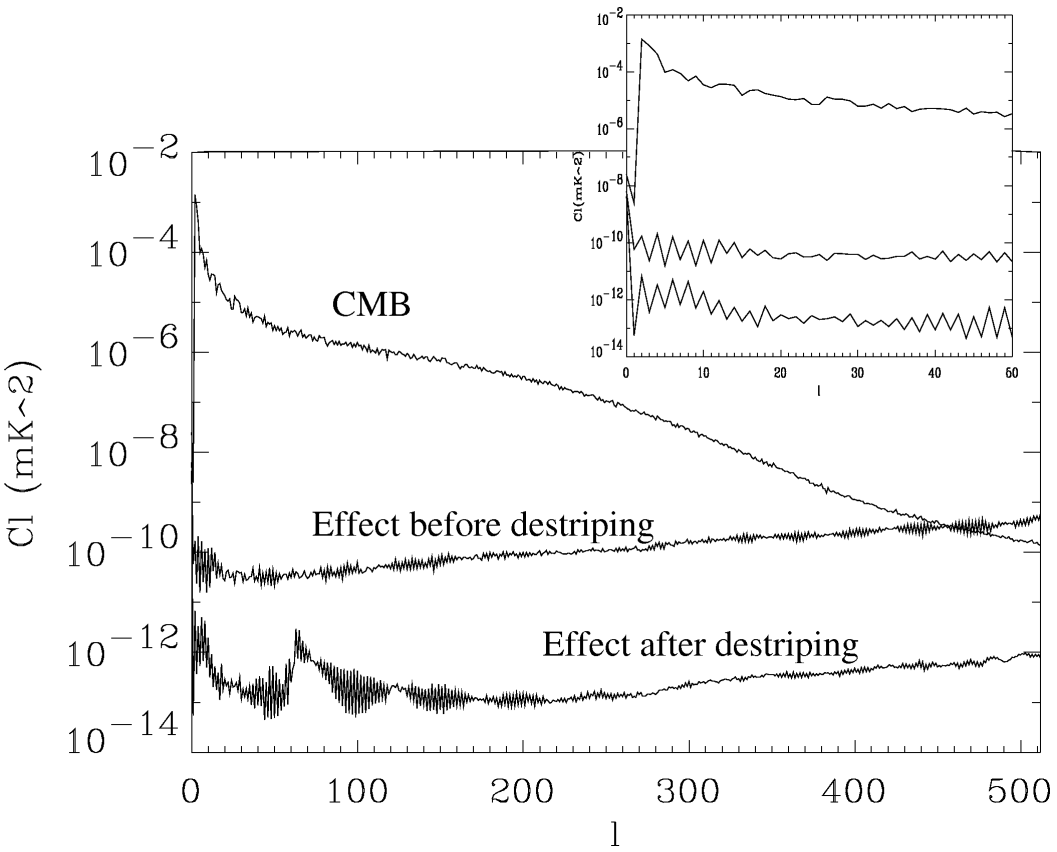

Figure 9 –Power spectra of the effect before and after destriping at 30 GHz (coupled scenario). A typical CMB power spectrum is plotted for comparison

In the following figures we show the same comparison for the 70 GHz case. In Figure 11 it is interesting to notice the rise in power spectrum at high multipoles that is characteristic of slow periodic effects mapped with a high angular resolution. In fact when time ordered data of "slow" periodic effects are coadded over the 60 repetitions of each sky ring, the resulting coadded TOD is a sequence of slopes with sharp discontinuities between adjacent circles. These discontinuities are responsible of the sharp power spectrum rise shown in Figure 11.

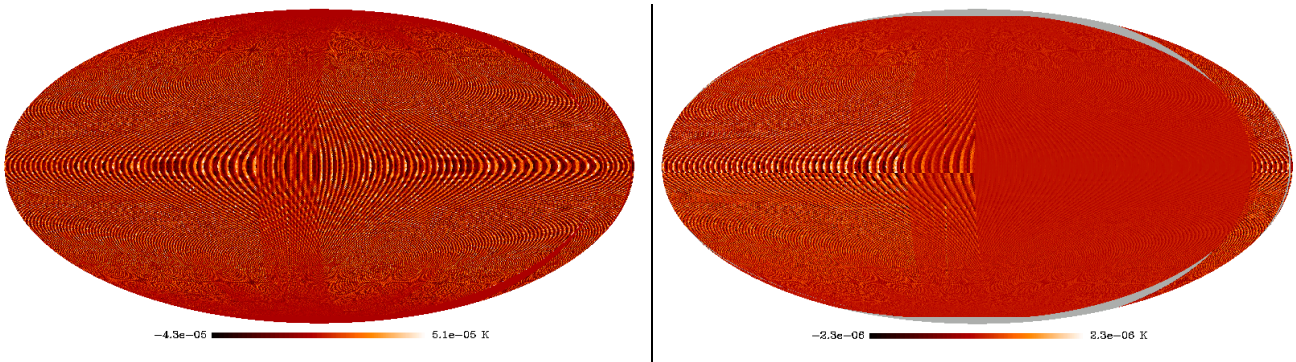

Figure 10 – Maps before and after destriping of the effect induced by fluctuations of the 4K reference load in the coupled scenario at 70 GHz

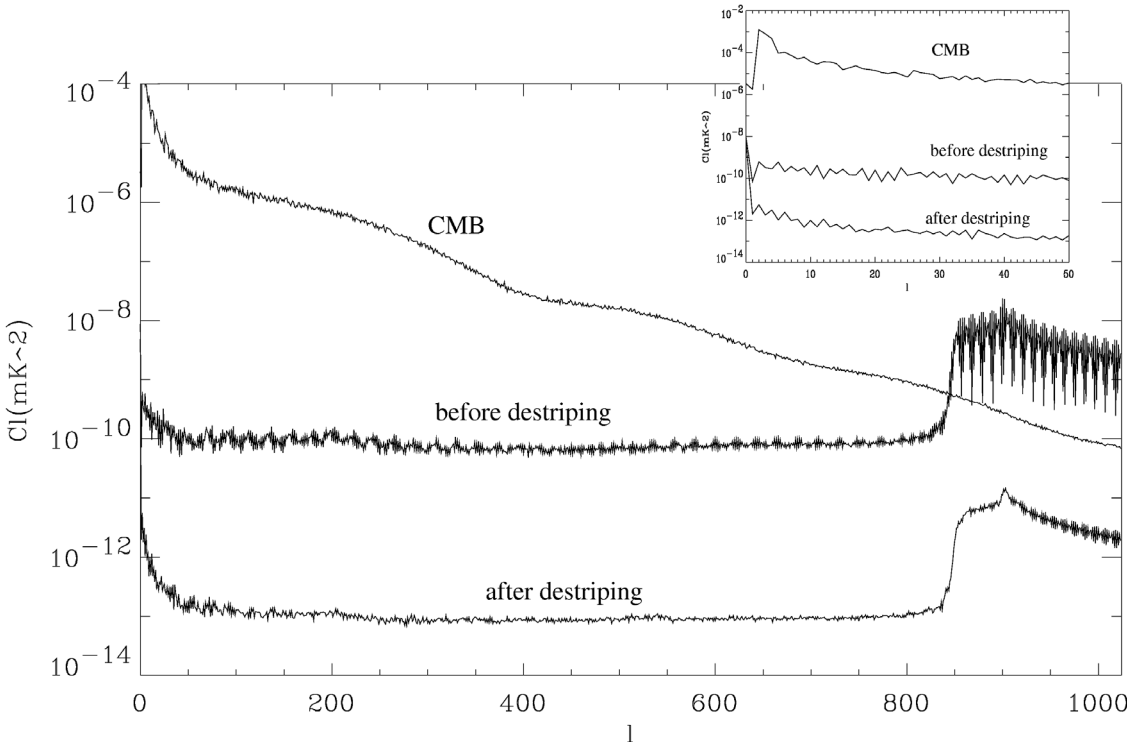

Figure 11 –Power spectra of the effect before and after destriping at 70 GHz (coupled scenario). A typical CMB power spectrum is plotted for comparison. Note the rise in the power spectrum of the effect at high multipole values (l > 800)

6. Conclusions

In this technical note we have discussed a preliminary evaluation of the effect of temperature fluctuations in the LFI 4K reference loads on the LFI measurements. The analysis considers the expected temperature variations at the interface between the reference loads and the HFI 4K box caused by the instability of the 4K cooler cold-end driven by the 18K stage temperature fluctuations.

Temperature data measured at the LR1 cold-end on the EBB sorption cooler have been used together with damping factors of the HFI structure calculated with the HFI thermal model; a simple model of the thermal damping provided by the ECCOSORB loads has been used to evaluate the actual temperature fluctuation at the load extremity. The temperature variation has then been converted into antenna temperature assuming perfect emissivity in the ECCOSORB load.

The estimated signal variation at the radiometric output is of the order of ~ 0.8 mK peak to peak that translates into an error of the order of several tens of micro-K per pixel when projected onto the sky. By applying classical destriping algorithms the effect is reduced to a level of the order of ~ 1 – 2 μK peak-to-peak which is close to the allowed limit in the systematic error budget plan (~ 2.2 μK peak-to-peak per pixel including spin synchronous effects).

The angular power spectrum of the effect increases at high multipole values exceeding the CMB power spectrum for $l > 400$ in the 30 GHz case and for $l > 800$ in the 70 GHz case. If destriping is applied to the effect then the power spectrum is suppressed by about 2 – 3 order of magnitudes.

Although the effect does not seem to be at the level of a *show-stopper* it cannot be considered negligible and will be further investigated along three main directions:

- take into account also the temperature fluctuations of the 4K cooler itself (that have been neglected in this study) as soon as measurements will become available;
- a more accurate modelling of the effect on maps and power spectra (considering the addition of astrophysical signal and instrumental noise) and the application of alternative filtering-destriping codes to the time-ordered data;
- a more accurate modelling of the signal emitted by the reference load into the radiometer as a consequence of physical temperature fluctuations.

7. References

[1] M. Seiffert, A. Mennella, C. Buriana, et al., *1/f noise and other systematic effects in Planck-LFI radiometers*, A&A, 391, 1185-1197 (2002)

[2] A. Mennella, M. Bersanelli, M. Seiffert, et al., *Offset balancing in pseudo correlation radiometers for CMB measurements*, A&A, to be published (2003)

[3] M. Bersanelli, A. Mennella, *Planck-LFI design report*, PL-LFI-PST-RP-002 3.0, March 2002

[4] M. Bersanelli, M. Seiffert, R. Hoyland, and A. Mennella, *Planck-LFI Scientific Requirements*, PL-LFI-PST-SP-011 2.0, March 2003

[5] G. Morgante, *LFI active temperature control – a first analysis*, July 2002, memo available on LiveLink at: http://www.rssd.esa.int/llink/livelink/90238/LFI_temperature_sensors_-_preliminary_overview.pdf?func=doc.Fetch&nodeid=90238

[6] L. Terenzi, *LFI PID preliminary analysis*, November 2002, memo available on LiveLink at: http://www.rssd.esa.int/llink/livelink/137034/LFI_PID_preliminary_analysis.pdf?func=doc.Fetch&nodeid=137034

[7] G. Guyot, *HFI-LFI IAS thermal fluctuations modelling*, TE-PH111-200181-IAS 01, February 2003

[8] M. Tomasi, *Propagazione di fluttuazioni termiche nello strumento Planck-LFI* (Propagation of thermal fluctuations in Planck-LFI instrument), Thesis degree, University of Milan, 2002 (PACS code 95.85.b)

[9] A. Mennella, M. Bersanelli, C. Burigana, et al., *Planck: systematic effects induced by periodic fluctuations of arbitrary shape*, A&A, 384, 736-742 (2002)